Potency boost of a *Mycobacterium tuberculosis* dihydrofolate reductase inhibitor by multienzyme $F_{420}H_2$-dependent reduction

Wassihun Wedajo Aragaw[a,1], Brendon M. Lee[b,1], Xuan Yang[c,d], Matthew D. Zimmerman[a], Martin Gengenbacher[a,e], Véronique Dartois[a,e], Wai-Keung Chui[c], Colin J. Jackson[b,f,g,2], and Thomas Dick[a,e,h,i,2]

[a]Center for Discovery and Innovation, Hackensack Meridian Health, Nutley, NJ 07110; [b]Research School of Chemistry, The Australian National University, Acton 2601, Australia; [c]Department of Pharmacy, Faculty of Science, National University of Singapore, 117543 Singapore, Singapore; [d]Discovery Sciences R&D, Forward Pharmaceuticals Co., Ltd., 518057 Shenzhen, People's Republic of China; [e]Department of Medical Sciences, Hackensack Meridian School of Medicine, Nutley, NJ 07110; [f]Australian Research Council (ARC) Centre of Excellence in Peptide and Protein Science, Research School of Chemistry, The Australian National University, Acton 2601, Australia; [g]ARC Centre of Excellence in Synthetic Biology, Research School of Chemistry, The Australian National University, Acton 2601, Australia; [h]Department of Microbiology and Immunology, Georgetown University, Washington, DC 20007; and [i]Department of Microbiology and Immunology, Yong Loo Lin School of Medicine, National University of Singapore, 117545 Singapore, Singapore

Edited by William R. Jacobs Jr., Albert Einstein College of Medicine, Bronx, NY, and approved May 13, 2021 (received for review December 7, 2020)

Triaza-coumarin (TA-C) is a *Mycobacterium tuberculosis* (Mtb) dihydrofolate reductase (DHFR) inhibitor with an IC_{50} (half maximal inhibitory concentration) of ∼1 μM against the enzyme. Despite this moderate target inhibition, TA-C shows exquisite antimycobacterial activity (MIC_{50}, concentration inhibiting growth by 50% = 10 to 20 nM). Here, we investigated the mechanism underlying this potency disconnect. To confirm that TA-C targets DHFR and investigate its unusual potency pattern, we focused on resistance mechanisms. In Mtb, resistance to DHFR inhibitors is frequently associated with mutations in thymidylate synthase *thyA*, which sensitizes Mtb to DHFR inhibition, rather than in DHFR itself. We observed *thyA* mutations, consistent with TA-C interfering with the folate pathway. A second resistance mechanism involved biosynthesis of the redox coenzyme F_{420}. Thus, we hypothesized that TA-C may be metabolized by Mtb F_{420}–dependent oxidoreductases (FDORs). By chemically blocking the putative site of FDOR-mediated reduction in TA-C, we reproduced the F_{420}-dependent resistance phenotype, suggesting that $F_{420}H_2$-dependent reduction is required for TA-C to exert its potent antibacterial activity. Indeed, chemically synthesized TA-C-Acid, the putative product of TA-C reduction, displayed a 100-fold lower IC_{50} against DHFR. Screening seven recombinant Mtb FDORs revealed that at least two of these enzymes reduce TA-C. This redundancy in activation explains why no mutations in the activating enzymes were identified in the resistance screen. Analysis of the reaction products confirmed that FDORs reduce TA-C at the predicted site, yielding TA-C-Acid. This work demonstrates that intrabacterial metabolism converts TA-C, a moderately active "prodrug," into a 100-fold-more-potent DHFR inhibitor, thus explaining the disconnect between enzymatic and whole-cell activity.

Mycobacterium tuberculosis | DHFR | antibacterial | F420

Tuberculosis (TB) is a major infectious disease killer globally. It affected 10 million and killed 1.4 million people in 2019 alone (1). The predicted impact of the COVID-19 pandemic is an additional 190,000 TB deaths in 2020, and it is expected in the next 5 y that there will be up to a 20% increase in the global TB disease burden (2), stressing the critical need for new safe and effective drugs against the causative agent, *Mycobacterium tuberculosis* (Mtb). In addition, controlling multidrug-resistant TB (MDR-TB) presents a huge public health challenge (1).

Dihydrofolate reductase (DHFR) is a ubiquitous enzyme in bacteria, parasites, and humans. The protein catalyzes the NADPH-dependent conversion of dihydrofolate into tetrahydrofolate, a methyl group shuttle required for the synthesis of many cellular building blocks including thymidylate, purines, and certain amino acids. Several DHFR inhibitors are in clinical use for the treatment of various infectious diseases and cancer (3, 4). However, approved DHFR inhibitors have only weak or no activity against Mtb, and there are no DHFR inhibitors used clinically for the treatment of TB (5).

Recently, DHFR was clinically validated as a vulnerable Mtb target. The old TB drug *para*-aminosalicylic acid (PAS) was long thought to inhibit dihydropteroate synthase (DHPS, FolP), the first enzyme in the folate pathway. However, it was uncovered that PAS, a hydroxy analog of DHPS's substrate *para*-aminobenzoic acid, is a substrate of DHPS, which catalyzes the formation of hydroxy-dihydrofolate, which in turn inhibits DHFR (6–10). Thus, PAS is a prodrug that, upon metabolism by an enzyme of the folate pathway, is converted into a DHFR inhibitor.

With Mtb DHFR presenting an attractive target, the enzyme has been the subject of renewed drug discovery efforts (5, 11–13), reviewed recently by He et al. (14). A major hurdle encountered in many DHFR drug discovery programs consists in achieving selectivity toward human DHFR (14). Through ligand-based drug design starting from a Triazaspiro scaffold and a side chain extension approach, we previously identified selective inhibitors of Mtb DHFR (15). The most potent and selective analog resulted

Significance

Bacterial metabolism can cause intrinsic drug resistance but can also convert inactive parent drugs into bioactive derivatives, as is the case for several antimycobacterial prodrugs. Here, we show that the intrabacterial metabolism of a Mtb dihydrofolate reductase (DHFR) inhibitor with moderate affinity for its target boosts its on-target activity by two orders of magnitude. This is a "prodrug-like" antimycobacterial that possesses baseline activity in the absence of intracellular bioactivation. By elucidating the metabolic enhancement mechanism, we have provided the basis for the rational optimization of a class of DHFR inhibitors and uncovered an antibacterial drug discovery concept.

Author contributions: W.W.A., B.M.L., M.D.Z., M.G., V.D., C.J.J., and T.D. designed research; W.W.A., B.M.L., M.Z., and M.G. performed research; W.W.A., B.M.L., X.Y., M.D.Z., V.D., W.-K.C., C.J.J., and T.D. contributed new reagents/analytic tools; W.W.A., B.M.L., M.D.Z., M.G., V.D., C.J.J., and T.D. analyzed data; and W.W.A., B.M.L., X.Y., M.D.Z., M.G., V.D., W.-K.C., C.J.J., and T.D. wrote the paper.

The authors declare no competing interest.

This article is a PNAS Direct Submission.

[1]W.W.A. and B.M.L. contributed equally to this work.

[2]To whom correspondence may be addressed. Email: colin.jackson@anu.edu.au or thomas.dick@hmh-cdi.org.

This article contains supporting information online at https://www.pnas.org/lookup/suppl/doi:10.1073/pnas.2025172118/-/DCSupplemental.

Published June 14, 2021.

from attachment of a coumarin fragment to the triaza scaffold (Triazaspiro-Coumarin [TA-C]; Fig. 1). TA-C inhibited recombinant Mtb DHFR with an IC_{50} of ~1 μM and showed an acceptable selectivity index for the human enzyme (IC_{50} human DHFR/IC_{50} Mtb DHFR = 18). The selectivity indices for cytotoxicity (CC_{50} HepG2/MIC_{50}) and hemolysis (LC_{50} red blood cells/MIC_{50}) were >4,000. Surprisingly, TA-C exhibited excellent whole-cell activity against Mtb and its closely related vaccine strain *M. bovis* bacillus Calmette–Guérin (bacillus Calmette–Guérin), with a Minimum Inhibitory Concentration$_{50}$ (MIC_{50}, concentration inhibiting growth by 50%) of 10 to 20 nM. To confirm that TA-C's whole-cell activity was due to inhibition of DHFR, we overexpressed DHFR in bacillus Calmette–Guérin and showed that TA-C's MIC increased when DHFR intrabacterial concentration increased (15).

The whole-cell activity or MIC_{50} of TA-C is 50- to 100-fold higher than its IC_{50} against the isolated Mtb DHFR protein. Here, our aim was to confirm DHFR inhibition as the primary mechanism of action of TA-C and to shed light on the peculiar on-target/whole-cell potency disconnect. Resistance to the prodrug DHFR inhibitor PAS has been extensively studied and recently discussed in comprehensive reviews by Baughn and colleagues (4, 16). PAS resistance can emerge via multiple mechanisms that include preventing efficient bioactivation within the folate synthesis pathway, mitigating the impact of target inhibition, and limiting drug accumulation within the bacilli. A common mechanism, identified by transposon mutagenesis (17), isolation of spontaneous resistant mutants in vitro (18), and genetic works (19), is associated with mutations in *thyA*, one of the genes encoding thymidylate synthase. Thymidylate synthase is required for the methylene-tetrahydrofolate–dependent conversion of dUMP to dTMP. In most organisms, this reaction is performed by a ThyA-type thymidylate synthase that releases dihydrofolate following catalysis. Dihydrofolate must be reduced by DHFR to re-enter the folate metabolism. Mtb encodes a second, ThyX-type thymidylate synthase. ThyX regenerates tetrahydrofolate instead of dihydrofolate following catalysis. In contrast to ThyX-mediated conversion of dUMP to dTMP, ThyA-mediated conversion results in an increased demand for DHFR activity to provide sufficient levels of tetrahydrofolate and therefore sensitizes the pathway to DHFR inhibition. Loss-of-function mutations in *thyA* reduce the demand for DHFR activity and are therefore associated with decreased susceptibility to DHFR inhibitors (4, 10, 16, 17, 20). It is interesting to note that missense resistance mutations in the *dfrA* gene encoding DHFR have not been reported in Mtb. Amino acid alterations that would prevent inhibitor binding to the active site of DHFR are likely deleterious to overall enzymatic function and are thus not tolerated by the bacterium (21). Resistant mutant selection with direct (nonprodrug) Mtb DHFR inhibitors, although less studied, is consistent with the resistance mechanisms observed for PAS. Using the DHFR inhibitor THT1 identified in a chemogenomic approach, Mugumbate et al. measured a spontaneous in vitro resistance frequency of ~10^{-8}/CFU (colony forming unit) and resistance mutations mapped to *thyA* (22).

Given that TA-C is a direct DHFR inhibitor, we anticipated a low frequency of resistance largely mapping to *thyA*. Instead, TA-C–resistant Mtb and bacillus Calmette–Guérin colonies emerged at a high frequency, and resistance was mostly due to loss of activity of enzymes within the biosynthetic pathway for the redox coenzyme F_{420} (23). We have previously shown that F_{420} is essential for emergence of Mtb from dormancy (24), and F_{420}-dependent oxidoreductases (FDORs) are known to activate other Mtb prodrugs, such as pretomanid (PA-824) (25). Employing genetics, analogs of TA-C as chemical probes, as well as biochemical analyses, we show that TA-C indeed intercepts DHFR but is in fact converted by bacterial FDORs to a carboxylic acid analog with 100-fold increased on-DHFR–target activity.

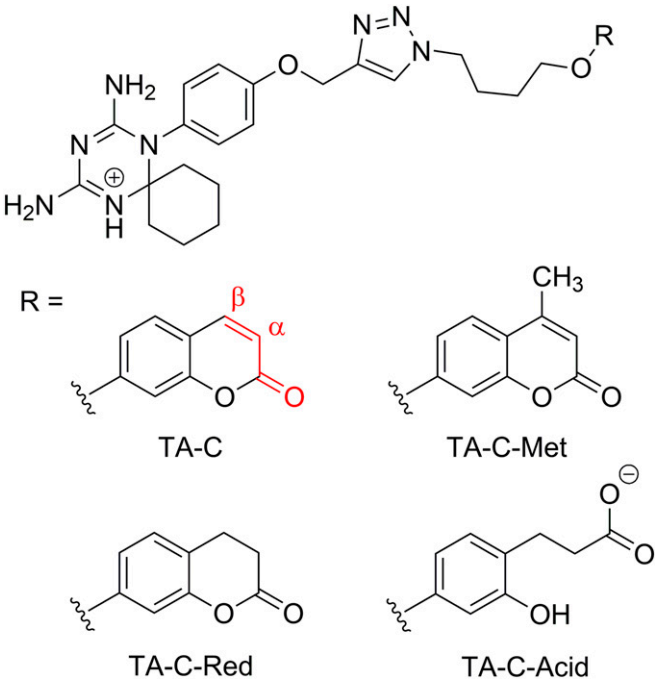

Fig. 1. Structure of TA-C and tool compounds TA-C-Met, TA-C-Red and TA-C-Acid. (*Above*) Triazaspiro core and linker common to TA-C and its analogs. (*Below*) coumarin moiety in TA-C (with α-β unsaturated carbonyl motif indicated in red), methylated coumarin in TA-C-Met, coumarin with reduced α-β double bond in TA-C-Red, and carboxylic acid derivative of coumarin in TA-C-Acid.

Results

High-Frequency TA-C Resistance Is Caused by Loss-of-Function Mutations in Genes Required for Synthesis of Redox Cofactor F_{420}. To identify TA-C resistance mechanisms, we selected spontaneous resistant mutants in bacillus Calmette–Guérin and Mtb on TA-C–containing agar. Surprisingly, resistant strains emerged at a high frequency of ~10^{-6}/CFU suggesting a TA-C–specific, nonfolate pathway–related resistance mechanism. MIC determination of 12 randomly selected resistant strains revealed a ~100-fold shift in MIC from 10 to 20 nM to 2 to 3 μM (Table 1). Consistent with a nonfolate pathway mechanism of resistance, all strains were fully susceptible to PAS. The MIC of isoniazid and rifampicin were not altered, suggesting that resistance to TA-C is specific and not due to a general drug resistance mechanism (Table 1). The 12 strains were subjected to whole-genome sequencing, and polymorphisms were verified by targeted sequencing. All strains harbored loss-of-function mutations in *fbiC* or *fbiA*, encoding the FO synthase and the F_{420}-L-glutamate ligase enzymes of the F_{420} biosynthetic pathway (23), and in *fgd1*, encoding the F_{420}-dependent glucose-6-phosphate dehydrogenase required for producing the reduced form of F_{420}, $F_{420}H_2$ (26) (Table 1). F_{420} is a deazaflavin cofactor involved in redox reactions in methanogens and many actinobacteria, including mycobacteria (23). Genetic complementation of representative strains harboring mutations in *fbiC*, *fbiA*, or *fgd1* restored wild-type TA-C susceptibility, confirming that TA-C resistance was caused by the observed polymorphisms (*SI Appendix*, Table S1). Measuring F_{420} contents in a representative mutant confirmed absence of the cofactor (*SI Appendix*, Fig. S1). Consistent with the loss of F_{420}, the 12 strains were cross-resistant to pretomanid (Table 1), a nitroimidazole prodrug bioactivated by the FDOR, deazaflavin-dependent reductase (Ddn) (27, 28). Thus, strains that are defective in F_{420} biosynthesis, F_{420} reduction, or prodrug activation are resistant to pretomanid (27, 29). In contrast to the analysis of resistant mutants selected against pretomanid, which identified Ddn (28), no FDOR was identified in our resistance screening. Together, these results

Table 1. TA-C–resistant *M. bovis* bacillus Calmette–Guérin and *M. tuberculosis* strains emerging at a frequency of 10^{-6}/CFU

			MIC$_{50}$ (μM)†								
	Exp*	Strain	TA-C	PAS	INH‡	RIF‡ (nM)	PTM‡	TA-C-Met	Gene with polymorphism	Mutation	Mutation type§
bacillus Calmette–Guérin		wt	0.02	0.8	0.4	1.6	0.2	3.2	—	—	—
	1	Tac^{r}1.1	3.2	0.8	0.4	2	>100	3.2	*fbiC*	Δ2269GC	fs
		Tac^{r}1.2	3.2	0.8	0.4	3	>100	3.2	*fgd1*	Δ472A	fs
		Tac^{r}1.3	3.2	0.8	0.4	2	>100	3.2	*fbiC*	Δ1142C	fs
	2	Tac^{r}2.1	1.6	0.4	0.3	1.6	>100	1.6	*fbiC*	Δ1983G	fs
		Tac^{r}2.2	3.2	0.4	0.4	1.6	>100	3.2	*fgd1*	Ins284C	fs
		Tac^{r}2.3	3.2	0.4	0.4	1.6	>100	3.2	*fbiA*	T326C, L109P	ms
	3	Tac^{r}3.1	3.2	0.8	0.3	3	>100	3.2	*fgd1*	Δ932A	fs
		Tac^{r}3.2	3.2	0.8	0.5	1.6	>100	3.2	*fbiC*	G928T, G310Stop	ns
		Tac^{r}3.3	3.2	0.4	0.4	1.6	>100	3.2	*fgd1*	C465A, Y155Stop	ns
Mtb		wt	0.01	0.2	0.4	1.6	0.2	1.6	—	—	—
	4	Tac^{r}4.1	1.6	0.2	0.4	1.6	>100	1.6	*fbiC*	Δ1084C	fs
	5	Tac^{r}5.1	1.6	0.2	0.4	1.6	>100	1.6	*fbiC*	Δ1976C	fs
	6	Tac^{r}6.1	1.6	0.2	0.4	1.6	>100	1.6	*fgd1*	T308G, L103R	ms

*Exp., independent resistance selection experiments.
†MIC experiments were carried out three times independently and mean values are shown.
‡INH, isoniazid; RIF, rifampicin; PTM, pretomanid.
§fs, frameshift; ms, missense; ns, nonsense mutation.

show that loss of F_{420} causes resistance to TA-C and that F_{420} is required for TA-C's potent whole-cell activity but did not identify exactly how F_{420} is involved in TA-C's activation.

Low-Frequency TA-C Resistance Is Caused by Missense and Nonsense Mutations in *thyA*. If TA-C indeed decreases folate synthesis by inhibiting DHFR, we expected TA-C–resistant mutants in folate metabolism genes at a frequency of ~10^{-8}/CFU (22). Thus, we speculated that out of 100 TA-C–resistant mutants emerging at a frequency of 10^{-6}/CFU, 99 should carry a defective F_{420} pathway, and one should harbor a mutation in the folate pathway. To test this hypothesis, we carried out a counter screen of a collection of 1,000 TA-C–resistant bacillus Calmette–Guérin strains for susceptibility to pretomanid. As expected, 994 strains were pretomanid resistant, presumably harboring lesions in F_{420} biosynthesis genes. The six TA-C–resistant and pretomanid-sensitive strains showed a ~100-fold increase in MIC$_{50}$ for TA-C (Table 2). Whole-genome sequencing, confirmed by targeted sequencing, revealed that all six strains carried missense or nonsense mutations in *thyA* (Table 2). Genetic complementation of a representative strain confirmed that a *thyA* polymorphism caused TA-C resistance (*SI Appendix*, Table S1). Furthermore, the *thyA* mutations conferred cross-resistance to PAS but not to the control drugs isoniazid and rifampicin (Table 2). Together, these results show that *thyA* mutations cause resistance to TA-C and emerge at a frequency of ~10^{-8}/CFU. These results suggest that the DHFR inhibitor TA-C exerts its antibacterial activity by interfering with folate metabolism.

Chemically Blocking the Putative TA-C Site of FDOR Reduction Phenocopies F_{420} Resistance. We first investigated whether F_{420} could be involved in the reduction of TA-C by FDORs, as is the case with nitroimidazole prodrugs, generating a derivative with enhanced antibacterial activity. Revisiting our published structure–activity relationship around the Triazaspiro scaffold, we noted that attachment of the coumarin group to the Triazaspiro core resulted in a moderate increase of biochemical activity and a strong increase of whole-cell activity (15). We speculated that TA-C's coumarin group may be the site of intrabacterial reduction by FDORs. It has been shown that the α,β-unsaturated carbonyl motif of coumarins can be reduced by enzymes within the FDOR superfamily (30–32). Thus, we hypothesized that Mtb FDORs reduce the coumarin moiety of TA-C, producing an activated derivative with increased whole-cell activity (Fig. 1). If correct, a TA-C analog in which this "reducible" site is blocked by chemical modification should copy the F_{420}-dependent resistance phenotype. To test this hypothesis, we generated the TA-C analog TA-C-Met, in which reducibility of the double bond was blocked by methylation of the β-carbon (Fig. 1) (30–32). TA-C-Met retained an IC$_{50}$ of ~1 μM against recombinant Mtb DHFR, similar to TA-C (Table 3). Thus, any altered whole-cell activity of TA-C-Met should be due to the loss of reduction since on-DHFR–target activity was preserved. As predicted, the MIC of TA-C-Met was ~100-fold higher compared to TA-C (Tables 1 and 3), around 2 to 3 μM, reproducing the TA-C resistance level of F_{420} mutants (Tables 1 and 3). Thus, the MIC of TA-C-Met was not affected by mutations causing loss of F_{420} (Tables 1 and 3). Together, these results indicate that TA-C is converted to an active derivative via FDOR-mediated reduction of the α,β-unsaturated carbonyl motif of its coumarin moiety and that F_{420}-associated resistance is due to the loss of TA-C reduction.

The Putative F_{420}-Dependent Reduction Product of TA-C, TA-C-Acid, Is a 10-nM DHFR Inhibitor. Analysis of the substrate range of FDORs with coumarin substrates has shown that reduction of the α,β-unsaturated carbonyl motif generates an unstable product that undergoes spontaneous ring opening by hydrolysis, which in turn releases a carboxylic acid coumarin derivative (30–32). Thus, we speculated that Mtb FDORs were the most likely enzyme class to carry out the analogous conversion of TA-C via a reduced intermediate (TA-C-Red) to generate TA-C-Acid (Fig. 1) and that TA-C-Acid may display increased activity against DHFR, thus explaining the enzyme/whole-cell potency disconnect. We synthesized TA-C-Acid and measured an IC$_{50}$ of ~10 nM against recombinant Mtb DHFR, showing that the putative reduction product of TA-C was 100-fold more potent than its parent against the enzyme (Table 3). Consistent with these biochemical results, structural modeling, in which TA-C and TA-C-Acid were computationally docked into the active site of Mtb DHFR (*SI Appendix*, Table S2 and Fig. S2), suggested that the carboxylic acid moiety of TA-C-Acid increases molecular interactions with the DHFR binding site, thus allowing tighter binding (Fig. 2 *A* and *B*).

The MIC$_{50}$ of TA-C-Acid was 0.8 μM against bacillus Calmette–Guérin, lower than the MIC$_{50}$ of TA-C-Met but significantly higher than the MIC of TA-C (Table 3). However, this is likely due to decreased intrabacterial uptake caused by the (charged)

Table 2. TA-C–resistant, pretomanid-sensitive *M. bovis* bacillus Calmette–Guérin strains emerging at a frequency of 10^{-8}/CFU

		MIC$_{50}$ (μM)[†]								
Exp*	Strain	TA-C	PTM[‡]	PAS	INH[‡]	RIF[‡] (nM)	TA-C-Met	Gene with polymorphism	Mutation	Mutation type[§]
	wt	0.02	0.2	0.8	0.4	1.6	3.2	—	—	—
7	Tac^{r}7.1	3.2	0.2	>100	0.4	1.6	3.2	*thyA*	C443A, A148E	ms
	Tac^{r}7.2	1.6	0.2	>100	0.4	1.6	3.2	*thyA*	G398C, W133S	ms
8	Tac^{r}8.1	1.6	0.2	>100	0.4	1.6	3.2	*thyA*	Ins734TATGAAG	ns
9	Tac^{r}9.1	3.2	0.2	>100	0.4	1.6	3.2	*thyA*	T373C, S125P	ms
10	Tac^{r}10.1	3.2	0.2	>100	0.4	1.6	3.2	*thyA*	C439T, H147Y	ms
	Tac^{r}10.2	3.2	0.2	>100	0.4	1.6	3.2	*thyA*	T292C, W98R	ms

*Exp., independent resistance selection experiments.
[†]MIC experiments were carried out three times independently and mean values are shown.
[‡]PTM, pretomanid; INH, isoniazid; RIF, rifampicin.
[§]ms, missense; ns, nonsense mutation.

carboxylic acid moiety (33). TA-C–resistant mutants in *thyA* and DHFR-overexpressing strains were both cross-resistant to TA-C-Acid, confirming that TA-C-Acid exerts its antibacterial activity by interfering with DHFR (Table 3).

Multiple Mtb F_{420} Oxidoreductases Reduce TA-C to TA-C-Acid. Results so far indicated that TA-C is a weak inhibitor of DHFR and is converted intracellularly by FDORs to the highly potent TA-C-Acid. However, the genetic screen for TA-C–resistant mutants revealed only loss-of-function mutations in genes involved in the F_{420} biosynthetic pathway and not in FDORs (Table 1). Thus, direct evidence for FDOR-catalyzed conversion of TA-C was missing. The Mtb genome encodes at least 28 F_{420}-dependent enzymes (34), 15 of which belong to the FDOR superfamily, including the nitroimidazole reductase responsible for pretomanid activation, Ddn (24). This enzyme family is known to be relatively promiscuous and active with a range of synthetic compounds (31, 32, 35–37). One explanation for the observation that no activating enzyme was detected in the resistance screen is that if multiple enzymes can activate the drug, they would all need to be inactivated to confer resistance (i.e., redundancy in activation can prevent evolution of resistance). If correct, this functional redundancy would explain our failure to isolate FDOR mutants resistant to TA-C.

To test this hypothesis, we screened a panel of seven recombinant FDORs from Mtb, including all members of the A1 subgroup that includes Ddn, as well as representatives of the A2, B1, B3, and B4 subgroups against TA-C using a spectrophotometric assay in which we followed the oxidation of $F_{420}H_2$ (*SI Appendix*, Table S3). We identified two enzymes from the A1 subgroup that could efficiently catalyze the reduction of TA-C in vitro, Ddn and Rv1558 (370 ± 14 and 152 ± 4 nmol $\cdot$ min^{-1} $\cdot$ umol$^{-1}_{\text{enzyme}}$, respectively) (*SI Appendix*, Table S3 and Fig. S3*A*). We also used the change in fluorescence of coumarin upon reduction to confirm that this apparent activity was a result of the reduction of the coumarinyl moiety (*SI Appendix*, Fig. S3*B*). We then measured the enzyme kinetics of Ddn and Rv1558 with TA-C revealing k_{cat}/K_M values of 1.71×10^3 M^{-1} $\cdot$ s^{-1} and 3.09×10^2 M^{-1} $\cdot$ s^{-1}, respectively (Table 3). To examine whether this promiscuous activity of FDORs with TA-C was likely to be common across other mycobacterial species, we also tested five recombinant enzymes from *Mycobacterium smegmatis,* identifying two (MSMEG_5998 and MSMEG_2027) that are orthologs of Ddn and Rv1558, respectively, from the A1 subgroup that had activity (*SI Appendix*, Table S3). Interestingly,

Table 3. The rate of reduction of TA-C, TA-C-Met, and TA-C-Acid by FDORs, their MIC$_{50}$ against *M. bovis* bacillus Calmette–Guérin, and IC$_{50}$ against DHFR*

	Compound		
Mtb FDOR Kinetics	TA-C	TA-C-Met	TA-C-Acid
Ddn	$5.95 \times 10^{-3} \pm 2.37 \times 10^{-4}$	N/D	N/D
k_{cat} (s^{-1})	3.47 ± 0.51	N/D	N/D
K_M (μM)	1.71×10^3	N/A	N/A
k_{cat}/K_M (M^{-1} s^{-1})			
Rv1558	$3.09 \times 10^{-3} \pm 1.48 \times 10^{-4}$	N/D	N/D
K_{cat} (s^{-1})	10.01 ± 1.6	N/D	N/D
k_M (μM)	3.09×10^2	N/A	N/A
k_{cat}/K_M (M^{-1} s^{-1})			
MIC$_{50}$ against bacillus Calmette–Guérin (μM)			
Wt	0.02	3.2	0.8
F_{420} mutant (Tac^{r}1.1)[†]	3.2	3.2	0.4
thyA mutant (Tac^{r}7.2)[†]	1.6	3.2	>25
DHFR over-expressor[§]	1.6	1.6	>25
DHFR IC$_{50}$ (μM)			
M. tuberculosis	0.93 ± 0.12	0.63 ± 0.07	0.009 ± 0.001
H. sapiens	10.5 ± 1.9	N/A	1.73 ± 0.14

N/D – Below the level of detection.
N/A – Not analyzed.
*Experiments were carried out three times independently and mean values are shown.
[†]Refer to Tables 1 and 2.
[§]Described in ref. 15.

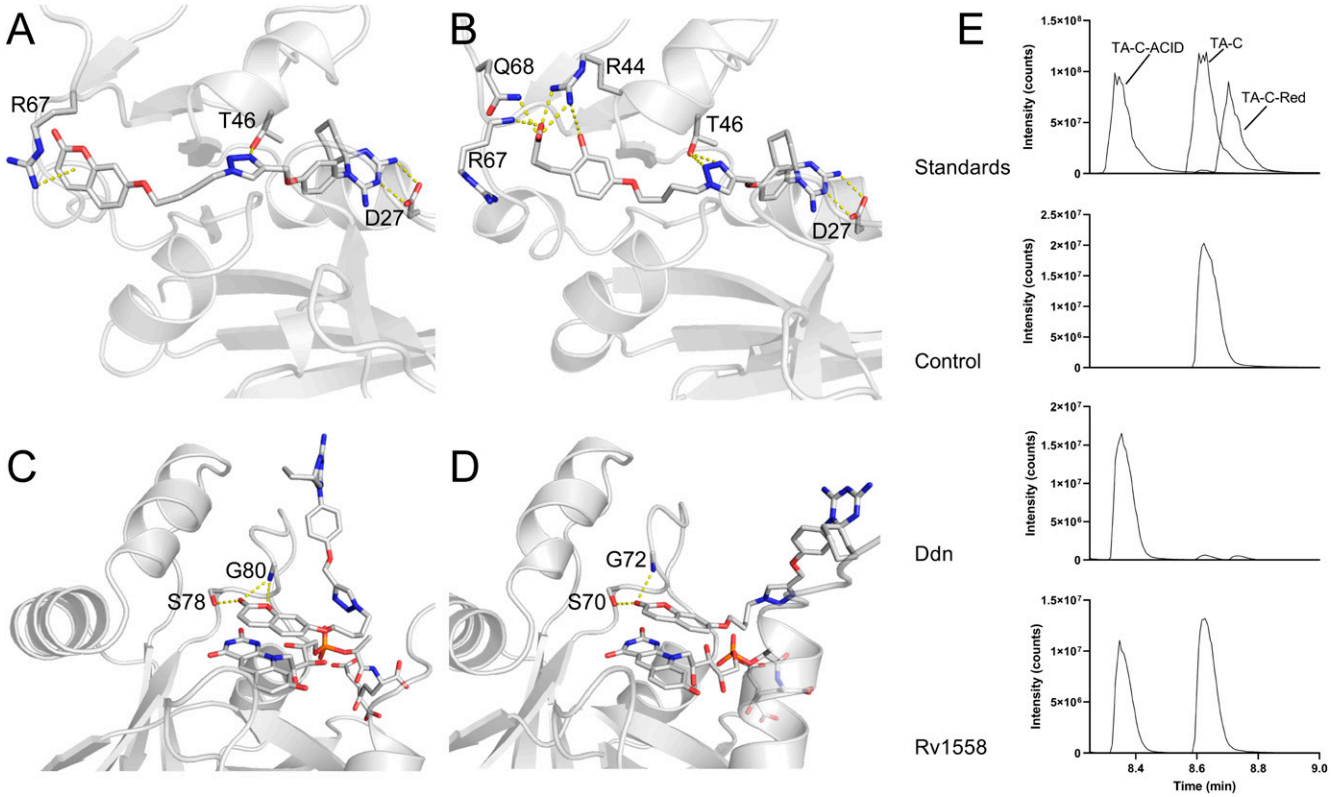

Fig. 2. TA-C docking analyses with DHFR and FDORs and conversion of TA-C by FDORs to TA-C-Acid. (*A*) TA-C docked into the binding pocket of DHFR (PDB ID: 6NND), with the cation–π interaction between R67 and the coumarin moiety highlighted. (*B*) TA-C-Acid docked into the binding pocket of DHFR, with the additional network of hydrogen bonds formed by the carboxylic acid moiety of TA-C-Acid and the sidechains of R67, Q68, and R44 highlighted. (*C*) TA-C bound into the binding pocket of Ddn:F_{420} (PDB ID: 3R5R), showing its stabilizing interactions with the main chain carbonyl and amide groups of S78 and G80. (*D*) TA-C bound into the binding pocket of Rv1558 with F_{420} (PDB ID: 7KL8), showing its stabilizing interactions with the main chain carbonyl and amide groups of S70 and G72. (*E*) LC/MS analysis of the Ddn and Rv1558 catalyzed conversion of TA-C to TA-C-Acid. No product formation was observed in the no-enzyme control sample.

the activity with TA-C appears to be limited to enzymes of the A1 subgroup, where Ddn and the 39% identical enzyme Rv1558 displayed significant activity. Despite reasonably high sequence identity (>34%), neither enzyme of the A2 subgroup (Rv1261c and MSMEG_5030) displayed activity. Because we could not obtain soluble, folded, and active protein for several of the FDORs, we cannot exclude the possibility that other enzymes in addition to Ddn and Rv1558 could activate TA-C. However, given the restricted activity to the A1 subgroup, the only plausible candidate is Rv3178, albeit unlikely given that it is less similar to Ddn than the inactive A2 enzymes (29% identity).

To investigate the activation of TA-C by these enzymes in more detail, we solved the structure of Rv1558, in complex with F_{420}, to a resolution of 2.47 Å (*SI Appendix*, Fig. S4 and Table S4). We were unable to capture the ternary complex between substrate, cofactor, and enzyme. As expected, Rv1558 adopts the split B-barrel fold typical of the FDOR superfamily (37) and is almost identical to the structure of Ddn at the level of the overall fold (rmsd C-α = 0.7 Å) (*SI Appendix*, Fig. S4). The N-terminal helix is fully resolved, unlike in the structure of Ddn, in which it is truncated. The active site is likewise very similar, with key catalytic residues such as Ser78, Tyr130, and Tyr136 (Ddn numbering) being conserved (38) and relatively conservative changes at other positions, such as Tyr65(Met) and Tyr130(Trp). TA-C was docked into the active sites of both proteins and adopts a catalytically productive pose (*SI Appendix*, Table S2 and Fig. S2), with the coumarin moiety positioned directly above the deazaflavin ring of F_{420} (Fig. 2 *C* and *D*). Triplicate 200-ns molecular dynamics simulations were then performed to confirm that these enzyme:-substrate complexes were stable over a reasonable timeframe for catalysis to occur (*SI Appendix*, Fig. S5). These findings provided direct biochemical and supporting structural evidence that TA-C is recognized as a substrate and metabolized by FDORs. The finding that at least two different FDORs accept TA-C as substrate explains the absence of TA-C–resistant strains harboring mutations in an FDOR. We also tested whether our tool compound TA-C-Met, in which reducibility of the α,β-unsaturated carbonyl motif was blocked, is metabolized by Ddn or Rv1558. As expected, TA-C-Met was not reduced by either enzyme, confirming that methylation of TA-C's coumarin motif blocks reduction (Table 3).

A key assumption of our model is that the Mtb FDORs Ddn and Rv1558 reduce the α,β-unsaturated carbonyl motif of TA-C's coumarin ring to produce TA-C-Red and that TA-C-Red undergoes spontaneous hydrolysis to TA-C-Acid as the reaction end product. Using chemically synthesized standards of TA-C, TA-C-Red, and TA-C-Acid, we followed the enzymatic conversion of TA-C to TA-C-Acid by Ddn and Rv1558 using liquid chromatography/mass spectrometry (LC/MS). In the case of Ddn, analysis of the reaction products revealed that the majority of the substrate (TA-C) has been converted to product after 1-h incubation, which had an *m/z* of 591.3 Da, consistent with TA-C-Acid. Two smaller peaks were present, one of which corresponded to the mass of the reduced intermediate species TA-C-Red, which had a *m/z* of 573.29 Da, consistent with the standard and with hydride transfer to the substrate peak (TA-C),

which had an *m/z* of TA-C (571.27 Da) (Fig. 2*E* and *SI Appendix*, Fig. S6). In the case of Rv1558, the conversion was slower, consistent with the enzyme kinetics (Table 3), and the intermediate peak was not observed; this would be expected if the spontaneous conversion of TA-C-Red to TA-C-Acid occurs more rapidly than the conversion of TA-C to TA-C-Red in this instance. Altogether, these results confirm that TA-C is indeed reduced by FDORs at the α,β-unsaturated carbonyl motif in TA-C's coumarin moiety and that the reduced form of TA-C spontaneously undergoes a ring-opening reaction to form TA-C-Acid as the end product.

To confirm that the conversion of TA-C to TA-C-Acid also occurs in intact bacteria, we treated *M. bovis* bacillus Calmette–Guérin culture with TA-C and observed time-dependent generation of TA-C-Acid with concurrent reduction of TA-C levels (*SI Appendix*, Fig. S7).

Previously, we showed that TA-C had specificity toward the Mtb DHFR over the human DHFR (15). Although the intracellular activation of TA-C within Mtb will greatly increase the specificity of this compound (25), we tested whether TA-C-Acid retained selectivity toward Mtb by testing its inhibition of human DHFR (Table 3). We observed that although TA-C-Acid inhibited human DHFR with greater affinity than TA-C (1.7 ± 0.1 versus 10.5 ± 1.9 μM, respectively), the increase in affinity was less than observed for the mycobacterial protein (Table 3). Thus, the FDOR-dependent activation of TA-C increases the selectivity to 188-fold for Mtb DHFR versus human DHFR.

To lay the ground for further compound optimization, we determined the pharmacokinetic (PK) profile of TA-C and TA-C-Acid following administration via the intravenous and oral routes. We observed no detectable oral bioavailability (*SI Appendix*, Fig. S8), which appears to be due to poor permeability, based on the intravenous PK profile and previously published in vitro PK data (15).

Discussion

Intrabacterial metabolism plays a prominent role in whole-cell activity—or inactivity—of antimycobacterials (39, 40). On one hand, intrabacterial drug metabolism can cause intrinsic drug resistance, which involves drug molecules that are active against isolated Mtb targets becoming converted into derivatives lacking the ability to engage their target once inside the bacterium. As an example, sulfonamides show potent activity against isolated Mtb DHPS but weak whole-cell activity because they are metabolized by Mtb (6). On the other hand, a number of highly successful antitubercular prodrugs, including the first-line drugs isoniazid and pyrazinamide, the second line drug PAS, and the newly approved pretomanid (6, 10, 27, 41, 42) do not have detectable activity against specific bacterial targets in their parent form but are converted by Mtb into derivatives with activity against intrabacterial targets. Here, we show that the Mtb DHFR inhibitor TA-C represents a category of antimycobacterial prodrug. In contrast to established Mtb prodrugs, TA-C was designed as a selective Mtb DHFR inhibitor and as such does exert biochemical activity against its target (15). However, upon uptake, Mtb converts TA-C to a more-selective and 100-fold more-potent DHFR inhibitor, TA-C-Acid (Fig. 3).

To characterize this prodrug paradigm, we isolated and analyzed spontaneous TA-C–resistant mutants in Mtb and bacillus Calmette–Guérin. Two types of resistance mechanisms were identified. As expected, TA-C resistance was caused by mutations in *thyA* at a frequency of ~10^{-8}/CFU (Table 3 and Fig. 3). *thyA* mutations are known to cause resistance to other DHFR inhibitors by reducing the vulnerability of folate synthesis and susceptibility of DHFR to chemical inhibition (4, 16). The second resistance mechanism was the loss of enzymes required for the biosynthesis of the redox cofactor F_{420} (Table 3 and Fig. 3). TA-C-Met, a TA-C analog in which FDOR-mediated reduction of the coumarin moiety is blocked, copied the F_{420}-resistance phenotype, suggesting that TA-C reduction by FDORs is required for full expression of antibacterial activity (Table 3 and Fig. 3). The putative product of FDOR reduction, TA-C-Acid, was 100-fold more potent against isolated Mtb DHFR (Table 3 and Fig. 3). Biochemical analyses using a collection of recombinant Mtb FDORs showed that at least two of these enzymes recognize TA-C as substrate, reduce the molecule at the predicted site, and generate TA-C-Acid (Table 3 and Fig. 3). This enhancement mechanism provides an explanation for the exquisite antibacterial activity of the DHFR inhibitor, which has an MIC_{50} of 10 to 20 nM despite moderate activity against its isolated target (Table 3). While these data are fully consistent with FDORs playing a role in activating TA-C, single- and double-knockout or overexpression strains of Ddn and Rv1558 were not generated and analyzed. Thus, one cannot unequivocally state that these two enzymes are indeed the FDORs responsible for the bioactivation of TA-C in intact bacteria.

TA-C in an F_{420}-deficient background and TA-C-Met in wild-type background, which are phenotypically equivalent, both retained appreciable whole-cell activity (MIC_{50} 2 to 3 μM), compatible with DHFR as their molecular target since both exhibit the same in vitro activity against DHFR (IC_{50} ~1 uM). However, TA-C-Met also retained the same activity in *thyA* mutants and DHFR-overexpressing strains (Table 3). This suggests that TA-C engages non-DHFR target(s) at this higher concentration. TA-C-Met–resistance selection experiments did not yield any resistant colonies up to 10^9 CFU of bacillus Calmette–Guérin. As TA-C–resistant mutations in *thyA* emerge at a frequency of ~10^{-8}/CFU, this low resistance frequency (<10^{-9}/CFU) 1) is consistent with a non-DHFR mechanism of action, which remains to be determined and 2) suggests that the compound engages more than one target and is not prone to (high-level) resistance development.

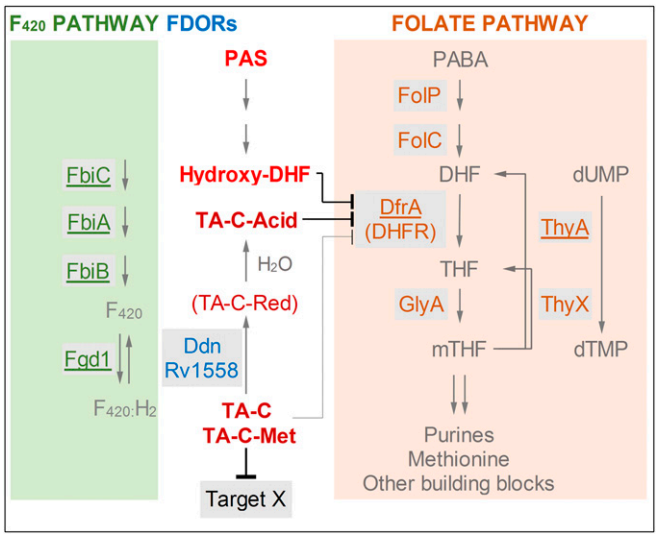

Fig. 3. F_{420} and folate pathways and mechanism of action of TA-C. Enzymes are indicated by gray background. Enzymes for which TA-C–resistant mutations were isolated are underlined (in the case of DfrA [DHFR], an engineered over-expressor strain conferred resistance). Metabolites are gray. TA-C and its derivatives are dark red. TA-C is converted by the FDORs Ddn and Rv1558 to TA-C-Red, which undergoes spontaneous hydrolysis to the highly potent DHFR inhibitor TA-C-Acid. The drug PAS is bright red. PAS is converted by FolP (DHPS) and FolC into the DHFR inhibitor hydroxy-DHF. Target X, unknown target(s) proposed to be intercepted by TA-C-Met and TA-C (*Discussion*). PABA, *para*-aminobenzoic acid; DHF, dihydrofolate; THF, tetrahydrofolate; and mTHF, methylene-tetrahydrofolate. The F_{420} pathway is according to Bashiri et al. (23). The folate pathway is according to Hajian et al. (8).

Rapid emergence of clinical resistance usually follows the clinical launch of drugs that target single enzymes, thus limiting their utility. A recent example is bedaquiline, approved by the US Food and Drug Administration in 2012 with clinical resistance reported shortly after its introduction (43, 44).

It may seem incongruous that the 2- to 3-μM antibacterial activity of TA-C-Met is not exerted via inhibition of DHFR despite an IC_{50} of ∼1 μM against the enzyme. However, most antibiotics inhibit their target at lower concentrations in biochemical assays than in bacterial cultures. Bedaquiline, which inhibits the F-ATP synthase with an IC_{50} of 2.5 nM, has an MIC of 54 nM, a 20-fold potency reduction from enzyme to whole cell (45). This common shift is associated with intrabacterial PK (uptake, metabolism, nonspecific binding to macromolecules, and efflux) resulting in lower free drug concentrations at the cellular site of the molecular target compared to the culture medium. Considering these observations, it is less surprising that TA-C-Met's inhibitory activity on the DHFR enzyme does not contribute to its 2- to 3-μM antibacterial activity.

In the same way that resistance can rapidly emerge against drugs that target a single protein, prodrugs are vulnerable to rapid evolution of resistance when a single activating enzyme is involved. For example, in the case of pretomanid, although we have shown that the fitness costs associated with mutations that cause loss of F_{420} biosynthesis are too great for this to become a widespread resistance mechanism, mutations that result in loss of the promiscuous prodrug-activating activity of Ddn, without substantially affecting the native menaquinone reductase activity, can cause resistance (and have already been detected in clinical samples) (24). TA-C is interesting in the context of those results because it is activated by multiple enzymes; the likelihood of Mtb becoming resistant via simultaneous mutations in multiple activating enzymes is extremely low. Thus, compounds such as TA-C, with multiple targets and multiple activating enzymes, represent an intriguing class of antimycobacterial compounds that could be resilient to the development of drug resistance.

In summary, we have demonstrated that TA-C, an antibacterial designed as a selective Mtb DHFR inhibitor, exerts its superb whole-cell antibacterial activity by disabling the folate pathway, albeit only after intrabacterial "bioaugmentation" by FDORs, explaining the unusual 100-fold boost from enzymatic to whole-cell activity. TA-C also appears to possess a DHFR-independent mechanism of action at low-μM concentrations, as revealed by its residual whole-cell activity in F_{420}-deficient strains and in *thyA* mutants resistant to DHFR inhibition. This multitargeting property of TA-C and the functional redundancy of the activating enzymes could be exploited through medicinal chemistry to mitigate the development of high-level resistance in future drug discovery programs.

Materials and Methods

Bacterial Strains, Media, and Culture Conditions. *M. bovis* bacillus Calmette–Guérin Pasteur (ATCC 35734) and *M. tuberculosis* H37Rv (ATCC 27294) were obtained from the American Type Culture Collection. Strains were grown in Middlebrook 7H9 broth (BD Difco) supplemented with 0.05% (vol/vol) Tween 80 (Sigma), 0.2% (vol/vol) glycerol (Fisher Scientific), and 10% (vol/vol) Middlebrook albumin-dextrose-catalase (BD Difco) at 37 °C with orbital shaking at 80 rpm. For determination of CFU, bacterial cultures were spread onto Middlebrook 7H11 agar (BD Difco) supplemented with 10% (vol/vol) Middlebrook oleic acid-albumin-dextrose-catalase and 0.2% glycerol and grown at 37 °C. When appropriate, agar was supplemented with TA-C or TA-C-Met for isolation of resistant mutants or 25 μg/mL kanamycin for the selection of transformed bacteria in the complementation experiments. *Escherichia coli* strains DH5-α and BL21 (DE3) were used for propagation of plasmids and expression of recombinant proteins, respectively, and were cultured in Luria–Bertani (LB) broth or on LB agar (BD Difco).

Chemicals. The synthesis of TA-C has been described previously (15). Synthesis of TA-C-Red is described in *SI Appendix, Supplementary Information*. TA-C-Met and TA-C-Acid were purchased from BioDuro. PAS, pretomanid, isoniazid, rifampicin, and kanamycin sulfate were purchased from Sigma-Aldrich. All drugs and chemicals were dissolved in 100% dimethyl sulfoxide (DMSO) at 10 mM except kanamycin, which was dissolved to 50 mg/mL in deionized water and sterilized using 0.2-μm Minisart high-flow syringe filters (Sartorius).

Selection of TA-C–Resistant Mutants. Mutant selection was carried out as described previously (46). In brief, bacterial inocula (∼10^6 to ∼10^8 CFU) from midlog cultures of *M. bovis* bacillus Calmette–Guérin or *M. tuberculosis* H37Rv were plated on 7H11 agar containing 3, 6, and 12 μM TA-C and grown for 4 wk at 37 °C. To verify resistance, colonies were picked and restreaked alongside wild-type bacteria on agar containing the TA-C concentrations on which the putative mutants were selected. Single colonies were picked from the restreak plates, inoculated into 7H9 broth, expanded to midlog phase, and stored with 10% glycerol at −80 °C until used for subsequent studies.

Counter Screen of TA-C–Resistant Mutants with Pretomanid. To identify TA-C–resistant strains that harbor a wild-type F_{420} pathway, we first isolated 1,000 TA-C–resistant *M. bovis* bacillus Calmette–Guérin strains and then identified the subset that is susceptible to pretomanid via replica plating (47). Briefly, 10 independently grown bacillus Calmette–Guérin cultures were plated onto 7H11 agar containing 3 μM TA-C and grown for 4 wk. Resistant colonies were picked, inoculated into 7H9 broth in flat-bottom 96-well plates and incubated for 7 d. The culture in each well was adjusted to an optical density at 600 nm (OD_{600}) = 0.1 and pin-plated onto 7H11 microplate agar dishes using a sterile 96-well pin replicator (Stem Corporation). Bacteria were spotted in duplicates on both drug-free and 20 μM pretomanid-containing agar. Wild-type bacillus Calmette–Guérin was included in each selection plate as control. TA-C–resistant colonies that did not grow on pretomanid agar were picked from the corresponding colony spots of drug-free replica plates, expanded in 7H9 broth to midlog phase, and stored with 10% glycerol at −80 °C.

MIC Determination. MIC were determined as described previously by generating growth inhibition dose–response curves (15). Briefly, drugs were serially diluted in flat-bottom 96-well plates, and a midlog-phase culture was mixed with the drug-containing broth (final OD_{600} = 0.005) and incubated for 10 d. Growth was monitored by measuring turbidity at 600 nm using a Tecan Infinite 200 Pro microplate reader (Tecan). MIC_{50}, the concentration that reduces growth by 50% compared to untreated control, was deduced from the generated dose–response curves.

Whole-Genome and Targeted Sequencing. Genomic DNA was extracted from bacillus Calmette–Guérin and Mtb strains using the phenol-chloroform method as described previously (46). Whole-genome sequencing was performed on the Illumina MiSeq platform. Library preparation (NEBNext Ultra kit, New England Biolabs), sequencing, and bioinformatic analyses were performed by AIT Biotech. To verify mutations, target genes were PCR amplified using custom-designed primers (*SI Appendix*, Table S6; Integrated DNA Technologies), and purified PCR products were Sanger sequenced (AIT Biotech).

Genetic Complementation Experiments. Representative TA-C–resistant *M. bovis* bacillus Calmette–Guérin mutants harboring polymorphisms in *fbiC*, *fbiA*, *fgd1*, or *thyA* were complemented with the respective wild-type copies of the genes. The coding sequences were PCR amplified from the bacillus Calmette–Guérin genome using custom primers (*SI Appendix*, Table S6) and fused to the hsp60 promoter in pMV262 (48). The expression cassettes composed of the hsp60 promoter and the respective coding sequence were transferred into the integrative plasmid pMV306 (41) as either *NotI*/*Eco*RI or *NotI*/*Hind*III fragments (*SI Appendix*, Table S5). After confirming the integrity of the constructs by sequencing (AIT Biotech), the plasmids were electroporated into bacillus Calmette–Guérin, and transformants were selected on kanamycin agar as described previously (49).

F_{420} Measurement. F_{420} contents of bacillus Calmette–Guérin cultures was determined by measuring crude cell extracts for F_{420}-specific fluorescence as described with minor modifications (50). In brief, late log-phase culture was harvested at OD_{600} = 1.0, washed in 0.9% (wt/vol) NaCl, and resuspended in disodium phosphate and potassium dihydrogen phosphate extraction buffer (50 mM each at pH = 5.7). The suspension was incubated in boiling water for 15 min, placed on ice for 10 min, and centrifuged at 13,000 × *g* for 40 min at 4 °C. To the supernatant, an equal volume of ice-cold 2-propanol was added, the mixture was spun (13,000 × *g* for 40 min at 4 °C), and the supernatant was dispensed in triplicate into a black flat-bottom 96-well plate for measurement

MICROBIOLOGY

of fluorescence at an excitation of 400 nm and an emission of 470 nm using a microplate reader (Infinite 200 Pro, Tecan). Statistical difference was compared with the wild-type fluorescence level using unpaired Studetn's *t* test (GraphPad Prism 8).

Cloning, Expression, and Purification of Enzymes (FDORs and DHFR). The *E. coli* codon-optimized sequences of Rv1261, Rv3178, and Rv1558 from *M. tuberculosis* were purchased as gene blocks from Integrated DNA Technologies and cloned into the expression vector pMAL-c2X using Gibson assembly (51). The Rv1558 sequence contained an N terminus His-tag and tev cleavage site between the maltose binding protein (MBP) tag and the protein. Codon-optimized Mtb DHFR coding sequence (Integrated DNA Technologies) was amplified using primers 5′-CGGCCATGGTGGGGCTGATCTGGG-3′ and 5′-CCG GAATTCTCATGAGCGGTGATAGGAGTA-3′. PCR products were digested with *Nco*I and *Eco*RI and cloned into pET-30a(+) plasmid (Novagen) digested with the same restriction enzymes. The recombinant plasmid was constructed such that an N terminally 6× histidine-tagged fusion protein is produced. The construction of plasmids for the heterologous production of the FDORs in *E. coli* has been previously described: Ddn (Rv3547) was expressed from pMAL-c2X (24), while all FDORs were expressed from pETMCSIII (Rv1155, Rv2074, Rv2991, MSMEG_2027, MSMEG_5998, MSMEG_6526, MSMEG_0048, MSMEG_2850, MSMEG_3356, MSMEG_3909, MSMEG_5030, and MSMEG_5215) (37). F_{420}-dependent glucose-6-phosphate dehydrogenase (FGD) was expressed from pDEST17 (52).

All proteins were expressed by transformation into *E. coli* (BL21 DE3) and grown on LB agar containing 50 μg/mL kanamycin or 100 μg/mL ampicillin. Single colonies were picked and inoculated in LB media with 50 μg/mL kanamycin or 100 μg/mL ampicillin and grown overnight at 37 °C. Starter cultures for DHFR, Ddn, Rv1261, Rv3178, and Rv1558 were diluted 1/100 in LB media containing 50 μg/mL kanamycin or 100 μg/mL ampicillin and grown at 37 °C until OD = 0.4. Cultures were induced with isopropyl β-d-1-thiogalactopyranoside (IPTG) to a final concentration of 0.3 mM and grown for 3 h or overnight at 25 °C. Starter cultures for all other proteins used in this study were diluted 1/100 in autoinduction media (20 g/l tryptone, 5 g/l yeast extract, 5 g/l NaCl, 6 g/l Na_2HPO_4, 3 g/l KH_2PO_4, 6 mL/l glycerol, 2 g/l lactose, 0.5 g/l glucose, and100 mg/mL ampicillin) and grown at 30 °C overnight. Cells were harvested by centrifugation at 8,500 × *g* for 20 min at 4 °C.

Proteins that were purified using the MBP tag (Ddn, Rv1261, Rv3178, and Rv1558) were resuspended in lysis buffer (20 mM Tris-Cl, pH = 7.5, 200 mM NaCl) and lysed by sonication using an Omni Sonicator Ruptor 400 (2 × 6 min at 50% power). The soluble extract was obtained by centrifugation at 13,500 × *g* for 1 h at 4 °C and filtered. The protein was purified by passing the lysate over amylose resin (NEB) and washed with lysis buffer. The protein was eluted using elution buffer (lysis buffer with 10 mM maltose). Samples were flash frozen and stored at −80 °C in 20 mM Tris pH = 7.5, 200 mM NaCl, 10 mM maltose, and 10% glycerol. All other proteins used in this study were purified using a His-tag and were resuspended in lysis buffer (50 mM $NaPO_4$, pH = 8, 300 mM NaCl, and 25 mM imidazole) and lysed by sonication as above. The soluble extract was obtained by centrifugation at 13,500 × *g* for 1 h at 4 °C, filtered and loaded 5-mL HisTrap HP column (GE Healthcare), and washed with lysis buffer. The protein was eluted with elution buffer (lysis buffer with 250 mM imidazole). Purified protein was passed through a GE HiPrep 26/10 desalting column for buffer exchange into 50 mM Tris-Cl, pH = 7, and 150 mM NaCl. Samples were flash frozen with 10% glycerol and stored at −80 °C. Rv1558 used for crystallography was further purified by removing the MBP and His-tag using tev protease at a 1:10 ratio and left overnight at 4 °C. Tag-free protein was purified by passing the TEV reaction over a 5-mL HisTrap HP column collecting the flow through. The collected protein was incubated with 1.5-fold excess F_{420} overnight at 4 °C, followed by size-exclusion chromatography on a GE Hiload 16/600 Superdex 75-pg column in buffer containing 20 mM Hepes pH = 7.5 and 150 mM NaCl. Fractions that were yellow and contained protein as identified by sodium dodecyl sulphate–polyacrylamide gel electrophoresis (SDS-PAGE) were pooled and used for crystallography after the sample diluted was in 20 mM Hepes pH = 7.5 to a final solution of in 20 mM Hepes pH = 7.5 and 50 mM NaCl and concentrated to 10 mg/mL.

F_{420} Purification. F_{420} was overexpressed and purified from *M. smegmatis* as previously described (53, 54). Briefly, *M. smegmatis* (mc^24517) cells were transformed with pYUBDuet-fbiABC by electroporation, plated on LB agar plates containing 0.05% Tween 80 and 50 μg/mL each hygromycin B and kanamycin and incubated at 37 °C for 3 d. Single colonies were picked and inoculated in LB media containing 0.05% Tween 80 and 50 μg/mL each hygromycin B and kanamycin and grown at 37 °C for 3 d. Starter cultures were diluted 1/100 into autoinduction media as described above and grown at 37 °C for 5 d. Cells were harvested by centrifugation at 10,000 × *g* for 30 min at 4 °C and resuspended in 20 mM Tris, pH = 7.5, and lysed by autoclave at 121 °C for 20 min. The soluble fraction was collected by centrifugation at 20,000 × *g* for 1 h at 4 °C. F_{420} was purified by passing the filtered lysate on a 60-mL Macroprep High-Q ion-exchange column (Bio-Rad). Fractions containing F_{420} identified by the presence of an absorption peak at 420 nm were collected and passed on a 75-mL hypersep C18 gravity column (Thermo Fisher), and F_{420} was eluted with 20% Methanol, freeze dried, and stored at −80 °C.

Enzyme Activity Assays. F_{420} was reduced overnight with 10 μM FGD and 10 mM glucose-6-phosphate in 20 mM Tris, pH = 7.5 under anaerobic conditions. FGD was removed by spin filtration in a 0.5-mL 10K molecular-weights cutoff (MWCO) spin filter (Millipore), and $F_{420}H_2$ was used within 1 h of FGD being removed. Enzyme assays with FDOR and TA-C were performed according to previously published methods (36, 37) in 50 mM Tris · HCl, pH = 7.5, 25 μM $F_{420}H_2$, 25 μM TA-C, and 1 μM enzyme at room temperature. Activity was monitored using fluorescence following the oxidation of $F_{420}H_2$ (excitation/emission: 400/470 nm). Specific enzyme activity of $F_{420}H_2$ oxidation was calculated using a standard curve of F_{420}.

LC/MS Assay. Enzymatic reactions for LC/MS analysis were done with 50 mM Tris pH = 7.5, 1 μM FGD, 5 μM F_{420}, 5 mM glucose-6-phosphate, 5 μM enzyme, and 25 μM TA-C for 1 h. All protein was removed by spin filtration in a 0.5-mL 10K MWCO spin filter (Millipore). Then, 1-μL aliquots were injected onto an ultimate 3000 ultrahigh performance liquid chromatography (UHPLC) coupled with an Orbitrap Elite (Thermo fisher). Samples were separated on an Agilent Eclipse XDB C18 column (1.8 μm, 2.1 × 50 mm) using the following gradient at 300 μL/min: 0 to 3 min 2% B, 3 to 8 min 2 to 80% B, 8 to 10 min 80% B, 10 to 10.5 min 80 to 2% B, and 10.5 to 15 min 2%, where A was 0.1% formic acid in MilliQ, and B was 0.1% formic acid in acetonitrile.

DHFR Inhibition Assay. Inhibition assays were done as previously described (15) with modification. All inhibition assays were performed in 150 mM potassium phosphate, pH = 7 containing 50 μM DHF, 60 μM NADPH, 10 nM DHFR, and 0 to 100 μM TA-C in 1/2 or 1/3 serial dilution. Enzyme velocity was determined by measuring the reduction of NADPH by absorbance at 340 nm for 10 min at room temperature using an Epoch microplate spectrophotometer (BioTek). Initial rates were corrected for nonenzymatic reduction, and enzymatic activity was determined using the NADPH extension coefficient (6,220 $M^{-1} \cdot cm^{-1}$). IC_{50} were calculated by fitting the percentage of inhibition by TA-C to a four-parameter sigmoidal dose–response curve using GraphPad Prism.

X-ray Crystallography. The Rv1558:F_{420} complex was screened for crystallization conditions by sitting vapor diffusion using SG1, PACT premier, JCSG-plus (Molecular Dimensions), and Peg/Ion HT (Hampton Research) high-throughput 96-well crystallization screens at 18 °C. The single crystal used for data collection was grown in 0.1 M sodium citrate pH = 5.8, 0.5 M ammonium sulfate, 1 M lithium sulfate, and 3% glycerol (vol/vol). The crystal was cryoprotected with the addition of 20% glycerol (vol/vol) and was flash cooled in liquid nitrogen. X-ray diffraction data were collected at the Australian Synchrotron beamline MX2. Diffraction data were indexed and integrated using X-ray detector software (XDS) (55) and scaled using AIMLESS (56). The structure was solved with molecular replacement in Molrep (57) using Ddn (PDB ID: 3R5R) (58) modified using CHAINSAW (59) as the search model. Model building, including manually modeling F_{420} into the difference density (mFo–DFc) at the binding site, was done with COOT (60) and refined using REFMAC (61). Models were optimized using the PDB_REDO server (62). Data collection and refinement statistics are provided in *SI Appendix*, Table S4.

Molecular Docking. Molecular docking was performed in the Schrödinger suite (Schrödinger release 2020-2, LLC). DHFR (PDB ID: 6NND) (63), Ddn with F_{420} (PDB ID: 3R5R) (58) and with a reconstructed N terminus as described previously (38), and Rv1558 with F_{420} (this study) were prepared in Protein Preparation Wizard (64). Briefly, any ligand present in the structure was removed, and each protein was preprocessed with bond order assigned, hydrogens added, waters removed, termini capped, and the ionization and tautomeric states of any het groups present were generated at pH = 7 using Epik. Het groups such as F_{420} were reviewed, and the lowest energy state with the appropriate bond order was chosen to use in the docking. Hydrogen bonds were assigned and optimized at pH = 7 using PROPKA (65), and the structure was optimized with restrained minimization using the OPLS3e force field (66). The structures of TA-C, TA-C-Met, and TA-C-Acid were created using ChemDraw (PerkinElmer Informatics) and prepared for docking by Ligprep (Schrödinger Release 2020-2: LigPrep, Schrödinger, LLC). Briefly, the ligands were minimalized using the OPLS3e force field. Ionization of the ligands were generated at pH = 7 using Epik, and each ligand retain their

specified chirality specified in the input files created from ChemDraw. All ligands were docked into each protein using Induced Fit Docking (67–69). A standard protocol was selected, and docking was performed using the OPLS3e force field. A 12-Å grid box was generated centered on the active site of each protein. Docking was performed with no constraints, ligands sampled ring conformation within an energy window of 2.5 kcal/mol, amide bonds were penalized for nonplanar conformations, and van der Waals radii scaling was set to 0.5. Residues that were within 5 Å of the docked ligand were refined using Prime with sidechains being optimized. Ligands within 30 kcal/mol of the best protein:ligand complex or within the top 20 were then redocked. The top 10 of each ligand:protein complex were analyzed, and the highest scoring result with an appropriate binding mode for either catalysis (Rv1558/Ddn) or inhibition (DHFR) was used for further analysis.

Molecular Dynamics. Molecular dynamics simulations were performed using Desmond (70), as implemented in the Schrödinger software suite (Schrödinger release 2020-2, LLC). The OPLS3e forcefield was used. The top-scoring docking complex of each structure with TA-C, TA-C-Met, or TA-C-Acid as described above were prepared in Protein Preparation Wizard (64) using the same settings as described above. Each protein was solvated in an orthorhombic box (10-Å buffer periodic boundary) with simple point-charge (SPC) water molecules, and the systems were neutralized using Na^+ or Cl^- ions. Following relaxation of the system, each simulation was run for 200 ns.

Data Availability. All study data are included in the article and/or *SI Appendix*.

ACKNOWLEDGMENTS. We thank Yoshiyuki Yamada, National University of Singapore, for help with cloning of Mtb DHFR. Research reported in this publication is supported by the National Institute of Allergy and Infectious Diseases of the NIH under Award R01AI132374. The content is solely the responsibility of the authors and does not necessarily represent the official views of the NIH. This work was also supported by the Singapore Ministry of Health's National Medical Research Council under Grant NMRC/TCR/011-NUHS/2014 as part of the Singapore Programme of Research Investigating New Approaches to Treatment of Tuberculosis led by Nick Paton and by the National Health Medical Research Council (NHMRC) project (Grant APP1139832), the ARC Centre of Excellence in Peptide and Protein Science (Grant CE200100012), and the ARC Centre of Excellence in Synthetic Biology (Grant CE200100029) to C.J.J., and the National University of Singapore Academic Research Fund Tier 1 Grant R-148-000-205-112 to W.-K.C. for the synthesis of the compounds. W.W.A. received a research scholarship from Singapore International Graduate Award.

1. WHO, *Global tuberculosis report 2020* (World Health Organization, Geneva, 2020).
2. P. Glaziou, Predicted impact of the COVID-19 pandemic on global tuberculosis deaths in 2020. *medRxiv* [Preprint] (2020). https://doi.org/10.1101/2020.04.28.20079582 (Accessed 13 September 2020).
3. I. M. Kompis, K. Islam, R. L. Then, DNA and RNA synthesis: Antifolates. *Chem. Rev.* **105**, 593–620 (2005).
4. S. L. Kordus, A. D. Baughn, Revitalizing antifolates through understanding mechanisms that govern susceptibility and resistance. *MedChemComm* **10**, 880–895 (2019).
5. M. R. Nixon *et al*., Folate pathway disruption leads to critical disruption of methionine derivatives in *Mycobacterium tuberculosis*. *Chem. Biol.* **21**, 819–830 (2014).
6. S. Chakraborty, T. Gruber, C. E. Barry III, H. I. Boshoff, K. Y. Rhee, Para-aminosalicylic acid acts as an alternative substrate of folate metabolism in *Mycobacterium tuberculosis*. *Science* **339**, 88–91 (2013).
7. S. Dawadi, S. L. Kordus, A. D. Baughn, C. C. Aldrich, Synthesis and analysis of bacterial folate metabolism intermediates and antifolates. *Org. Lett.* **19**, 5220–5223 (2017).
8. B. Hajian *et al*., Drugging the folate pathway in Mycobacterium tuberculosis: the role of multi-targeting agents. *Cell Chem. Biol.* **26**, 781–791.e6 (2019).
9. F. Zhao *et al*., Binding pocket alterations in dihydrofolate synthase confer resistance to para-aminosalicylic acid in clinical isolates of *Mycobacterium tuberculosis*. *Antimicrob. Agents Chemother.* **58**, 1479–1487 (2014).
10. J. Zheng *et al*., para-Aminosalicylic acid is a prodrug targeting dihydrofolate reductase in *Mycobacterium tuberculosis*. *J. Biol. Chem.* **288**, 23447–23456 (2013).
11. A. B. Gerum *et al*., Novel *Saccharomyces cerevisiae* screen identifies WR99210 analogues that inhibit *Mycobacterium tuberculosis* dihydrofolate reductase. *Antimicrob. Agents Chemother.* **46**, 3362–3369 (2002).
12. A. Kumar *et al*., A focused screen identifies antifolates with activity on *Mycobacterium tuberculosis*. *ACS Infect. Dis.* **1**, 604–614 (2015).
13. A. Kumar *et al*., High-throughput screening and sensitized bacteria identify an *M. tuberculosis* dihydrofolate reductase inhibitor with whole cell activity. *PLoS One* **7**, e39961 (2012).
14. J. He, W. Qiao, Q. An, T. Yang, Y. Luo, Dihydrofolate reductase inhibitors for use as antimicrobial agents. *Eur. J. Med. Chem.* **195**, 112268 (2020).
15. X. Yang *et al*., 1,3,5-triazaspiro[5.5]undeca-2,4-dienes as selective *Mycobacterium tuberculosis* dihydrofolate reductase inhibitors with potent whole cell activity. *Eur. J. Med. Chem.* **144**, 262–276 (2018).
16. Y. Minato *et al*., *Mycobacterium tuberculosis* folate metabolism and the mechanistic basis for para-aminosalicylic acid susceptibility and resistance. *Antimicrob. Agents Chemother.* **59**, 5097–5106 (2015).
17. J. Rengarajan *et al*., The folate pathway is a target for resistance to the drug para-aminosalicylic acid (PAS) in mycobacteria. *Mol. Microbiol.* **53**, 275–282 (2004).
18. V. Mathys *et al*., Molecular genetics of para-aminosalicylic acid resistance in clinical isolates and spontaneous mutants of *Mycobacterium tuberculosis*. *Antimicrob. Agents Chemother.* **53**, 2100–2109 (2009).
19. A. S. Fivian-Hughes, J. Houghton, E. O. Davis, *Mycobacterium tuberculosis* thymidylate synthase gene *thyX* is essential and potentially bifunctional, while *thyA* deletion confers resistance to p-aminosalicylic acid. *Microbiology (Reading)* **158**, 308–318 (2012).
20. A. F. Schober *et al*., A two-enzyme adaptive unit within bacterial folate metabolism. *Cell Rep.* **27**, 3359–3370.e7 (2019).
21. J. V. Rodrigues *et al*., Biophysical principles predict fitness landscapes of drug resistance. *Proc. Natl. Acad. Sci. U.S.A.* **113**, E1470–E1478 (2016).
22. G. Mugumbate *et al*., Mycobacterial dihydrofolate reductase inhibitors identified using chemogenomic methods and in vitro validation. *PLoS One* **10**, e0121492 (2015).
23. G. Bashiri *et al*., A revised biosynthetic pathway for the cofactor F_{420} in prokaryotes. *Nat. Commun.* **10**, 1558 (2019).
24. B. M. Lee *et al*., Predicting nitroimidazole antibiotic resistance mutations in *Mycobacterium tuberculosis* with protein engineering. *PLoS Pathog.* **16**, e1008287 (2020).
25. R. Singh *et al*., PA-824 kills nonreplicating *Mycobacterium tuberculosis* by intracellular NO release. *Science* **322**, 1392–1395 (2008).
26. E. Purwantini, L. Daniels, Molecular analysis of the gene encoding F_{420}-dependent glucose-6-phosphate dehydrogenase from *Mycobacterium smegmatis*. *J. Bacteriol.* **180**, 2212–2219 (1998).
27. C. K. Stover *et al*., A small-molecule nitroimidazopyran drug candidate for the treatment of tuberculosis. *Nature* **405**, 962–966 (2000).
28. U. H. Manjunatha *et al*., Identification of a nitroimidazo-oxazine-specific protein involved in PA-824 resistance in *Mycobacterium tuberculosis*. *Proc. Natl. Acad. Sci. U.S.A.* **103**, 431–436 (2006).
29. H. L. Haver *et al*., Mutations in genes for the F_{420} biosynthetic pathway and a nitroreductase enzyme are the primary resistance determinants in spontaneous in vitro-selected PA-824-resistant mutants of *Mycobacterium tuberculosis*. *Antimicrob. Agents Chemother.* **59**, 5316–5323 (2015).
30. M. C. Taylor *et al*., Identification and characterization of two families of F_{420} H_2-dependent reductases from Mycobacteria that catalyse aflatoxin degradation. *Mol. Microbiol.* **78**, 561–575 (2010).
31. G. V. Lapalikar *et al*., $F_{420}H_2$-dependent degradation of aflatoxin and other furanocoumarins is widespread throughout the actinomycetales. *PLoS One* **7**, e30114 (2012).
32. C. Greening *et al*., Mycobacterial $F_{420}H_2$-dependent reductases promiscuously reduce diverse compounds through a common mechanism. *Front. Microbiol.* **8**, 1000 (2017).
33. M. F. Richter *et al*., Predictive compound accumulation rules yield a broad-spectrum antibiotic. *Nature* **545**, 299–304 (2017).
34. J. D. Selengut, D. H. Haft, Unexpected abundance of coenzyme $F(_{420})$-dependent enzymes in *Mycobacterium tuberculosis* and other actinobacteria. *J. Bacteriol.* **192**, 5788–5798 (2010).
35. G. V. Lapalikar *et al*., Cofactor promiscuity among F_{420}-dependent reductases enables them to catalyse both oxidation and reduction of the same substrate. *Catal. Sci. Technol.* **2**, 1560–1567 (2012).
36. T. Jirapanjawat *et al*., The redox cofactor F_{420} protects mycobacteria from diverse antimicrobial compounds and mediates a reductive detoxification system. *Appl. Environ. Microbiol.* **82**, 6810–6818 (2016).
37. F. H. Ahmed *et al*., Sequence–structure–function classification of a catalytically diverse oxidoreductase superfamily in Mycobacteria. *J. Mol. Biol.* **427**, 3554–3571 (2015).
38. A. E. Mohamed *et al*., Hydrophobic shielding drives catalysis of hydride transfer in a family of $F_{420}H_2$-dependent enzymes. *Biochemistry* **55**, 6908–6918 (2016).
39. A. V. Vasilevskaya *et al*., Identification of *Mycobacterium tuberculosis* enzyme involved in vitamin D and 7-dehydrocholesterol metabolism. *J. Steroid Biochem. Mol. Biol.* **169**, 202–209 (2017).
40. S. Luthra, A. Rominski, P. Sander, The role of antibiotic-target-modifying and antibiotic-modifying enzymes in *Mycobacterium abscessus* drug resistance. *Front. Microbiol.* **9**, 2179 (2018).
41. Y. Zhang, B. Heym, B. Allen, D. Young, S. Cole, The catalase-peroxidase gene and isoniazid resistance of *Mycobacterium tuberculosis*. *Nature* **358**, 591–593 (1992).
42. A. Scorpio, Y. Zhang, Mutations in *pncA*, a gene encoding pyrazinamidase/nicotinamidase, cause resistance to the antituberculous drug pyrazinamide in tubercle bacillus. *Nat. Med.* **2**, 662–667 (1996).
43. G. V. Bloemberg *et al*., Acquired resistance to bedaquiline and delamanid in therapy for tuberculosis. *N. Engl. J. Med.* **373**, 1986–1988 (2015).
44. S. Andres *et al*., Bedaquiline-resistant tuberculosis: Dark clouds on the horizon. *Am. J. Respir. Crit. Care Med.* **201**, 1564–1568 (2020).
45. J. Guillemont, C. Meyer, A. Poncelet, X. Bourdrez, K. Andries, Diarylquinolines, synthesis pathways and quantitative structure–Activity relationship studies leading to the discovery of TMC207. *Future Med. Chem.* **3**, 1345–1360 (2011).
46. P. Gopal *et al*., Pyrazinamide resistance is caused by two distinct mechanisms: Prevention of coenzyme A depletion and loss of virulence factor synthesis. *ACS Infect. Dis.* **2**, 616–626 (2016).
47. J. Lederberg, E. M. Lederberg, Replica plating and indirect selection of bacterial mutants. *J. Bacteriol.* **63**, 399–406 (1952).
48. C. K. Stover *et al*., New use of BCG for recombinant vaccines. *Nature* **351**, 456–460 (1991).

49. Y. Yamada, T. Dick, Mycobacterial caseinolytic protease gene regulator ClgR is a substrate of caseinolytic protease. *mSphere* **2**, e00338-16 (2017).
50. D. Guerra-Lopez, L. Daniels, M. Rawat, *Mycobacterium smegmatis* mc^2 155 *fbiC* and MSMEG_2392 are involved in triphenylmethane dye decolorization and coenzyme F_{420} biosynthesis. *Microbiology (Reading)* **153**, 2724–2732 (2007).
51. D. G. Gibson *et al*., Enzymatic assembly of DNA molecules up to several hundred kilobases. *Nat. Methods* **6**, 343–345 (2009).
52. G. Bashiri, C. J. Squire, N. J. Moreland, E. N. Baker, Crystal structures of F_{420}-dependent glucose-6-phosphate dehydrogenase FGD1 involved in the activation of the antituberculosis drug candidate PA-824 reveal the basis of coenzyme and substrate binding. *J. Biol. Chem.* **283**, 17531–17541 (2008).
53. G. Bashiri, A. M. Rehan, D. R. Greenwood, J. M. Dickson, E. N. Baker, Metabolic engineering of cofactor F_{420} production in *Mycobacterium smegmatis*. *PLoS One* **5**, e15803 (2010).
54. D. Isabelle, D. R. Simpson, L. Daniels, Large-scale production of coenzyme F_{420}-5,6 by using *Mycobacterium smegmatis*. *Appl. Environ. Microbiol.* **68**, 5750–5755 (2002).
55. W. Kabsch, XDS. *Acta Crystallogr. D Biol. Crystallogr.* **66**, 125–132 (2010).
56. P. R. Evans, G. N. Murshudov, How good are my data and what is the resolution? *Acta Crystallogr. D Biol. Crystallogr.* **69**, 1204–1214 (2013).
57. A. Vagin, A. Teplyakov, MOLREP: An automated program for molecular replacement. *J. Appl. Cryst.* **30**, 1022–1025 (1997).
58. S. E. Cellitti *et al*., Structure of Ddn, the deazaflavin-dependent nitroreductase from Mycobacterium tuberculosis involved in bioreductive activation of PA-824. *Structure* **20**, 101–112 (2012).
59. N. Stein, CHAINSAW: A program for mutating pdb files used as templates in molecular replacement. *J. Appl. Cryst.* **41**, 641–643 (2008).
60. P. Emsley, B. Lohkamp, W. G. Scott, K. Cowtan, Features and development of coot. *Acta Crystallogr. D Biol. Crystallogr.* **66**, 486–501 (2010).
61. G. N. Murshudov *et al*., REFMAC5 for the refinement of macromolecular crystal structures. *Acta Crystallogr. D Biol. Crystallogr.* **67**, 355–367 (2011).
62. R. P. Joosten, F. Long, G. N. Murshudov, A. Perrakis, The PDB_REDO server for macromolecular structure model optimization. *IUCrJ* **1**, 213–220 (2014).
63. J. A. Ribeiro *et al*., Crystal structures of the closed form of *Mycobacterium tuberculosis* dihydrofolate reductase in complex with dihydrofolate and antifolates. *Acta Crystallogr. D Struct. Biol.* **75**, 682–693 (2019).
64. G. M. Sastry, M. Adzhigirey, T. Day, R. Annabhimoju, W. Sherman, Protein and ligand preparation: Parameters, protocols, and influence on virtual screening enrichments. *J. Comput. Aided Mol. Des.* **27**, 221–234 (2013).
65. M. H. Olsson, C. R. Søndergaard, M. Rostkowski, J. H. Jensen, PROPKA3: consistent treatment of internal and surface residues in empirical p K a predictions. *J. Chem. Theory Comput.* **7**, 525–537 (2011).
66. K. Roos *et al*., OPLS3e: Extending force field coverage for drug-like small molecules. *J. Chem. Theory Comput.* **15**, 1863–1874 (2019).
67. W. Sherman, T. Day, M. P. Jacobson, R. A. Friesner, R. Farid, Novel procedure for modeling ligand/receptor induced fit effects. *J. Med. Chem.* **49**, 534–553 (2006).
68. W. Sherman, H. S. Beard, R. Farid, Use of an induced fit receptor structure in virtual screening. *Chem. Biol. Drug Des.* **67**, 83–84 (2006).
69. R. Farid, T. Day, R. A. Friesner, R. A. Pearlstein, New insights about HERG blockade obtained from protein modeling, potential energy mapping, and docking studies. *Bioorg. Med. Chem.* **14**, 3160–3173 (2006).
70. K. J. Bowers *et al*., "Scalable algorithms for molecular dynamics simulations on commodity clusters" in *SC'06: Proceedings of the 2006 ACM/IEEE Conference on Supercomputing*, B. Horner-Miller, Ed. (IEEE, Tampa, FL, 2006), p. 43.